İSTANBUL UNIVERSITY CERRAHPAŞA

ORIGINAL ARTICLE
Electrica 2024; 24(1): 25-38

Investigation of the Effect of Different Electromagnetic Interference Filter Topologies to DC–DC Boost Converter for Continuous Conduction Mode

Erdal Şehirli

Department of Electrical and Electronics Engineering, Kastamonu University Faculty of Engineering and Architecture, Kastamonu, Turkey

Cite this article as: E. Şehirli, "Investigation of the effect of different electromagnetic interference filter topologies to DC–DC boost converter for continuous conduction mode," *Electrica*, 24(1), 25-38, 2024.

ABSTRACT

This paper presents the design and application of boost converter operated in continuous conduction mode for 15 W, with 25 kHz switching frequency with induc tor-capacitor-inductor (LCL), pi, inductor capacitor (LC) with damping, and LC electromagnetic interference filters. Also, modeling and analysis of the boost converter in terms of state space and small signal are given. Furthermore, the effect of each filter to differential mode (DM) noise and to control characteristics by root locus and bode diagrams for the boost converter are presented, which is not presented in detail in the literature for the boost converter. All results obtained by applications and simulations are compared. Moreover, frequency spectrums are given to compare DM noises. As a result, for control point of view, LCL filter provides better results, and for reducing DM noise, the LC and pi filters are superior to others. Besides, the LCL filter reduces the inductor value by 30% compared to other filters.

***Index Terms*—**Boost, Differential Mode noise, Electromagnetic Interference filter, small signal

I. INTRODUCTION

The electromagnetic interference (EMI) filter issue is one of the most key topics in power electronics due to the high-frequency noises presented by power switches. Input sources may have voltage drops because of the high-frequency noises, and such noises disrupt the operation of other devices. Besides, using converters with higher-magnitude noises can harm solar panels in terms of renewable energy. Furthermore, noises with higher magnitude can arise at each operation of the power converter, including boundary conduction mode (BCM), discontinuous conduction mode (DCM), and continuous conduction mode (CCM), which inevitably have higher current ripples. Therefore, the design process of the EMI filter must be made carefully, especially for the DC–DC boost converter, which is the most preferable topology for maximum power extraction from solar panels.

The design, operation, and analysis of the boost converter are given in [1]. For power converters, EMI filter structures canceling differential mode (DM) noise are presented in [2-4]. The most popular topology for power converters is an inductor capacitor (LC) filter, whose design and analysis are given in [5-6]. Also, configurations and analysis of LC filters having damping circuits to provide damping to filter resonance are included in [2, 5-6]. Some applications use the pi filter as a DM filter in [7-8] without giving a detailed analysis of the filter effect on the boost converter. The design of the inductor-capacitor-inductor (LCL) filter is realized for inverter applications in [9], for boost converters in [10] without examining its effect on control characteristics. For the buck converter, the effect of the LC filter on the control characteristic is examined in [11-12] without considering DM noise. LC with damping and LC filter effect is investigated in [13] by cascading transfer functions of the boost converter and filters without comparing DM noise. For the boost converter, [14] derives small-signal analysis and modeling based on average state space. Also, a circuit-based average model for boost converter is given in [15-18] with small-signal analysis. In addition, the filter effect on the converter is analyzed in [19] for an isolated Cuk converter, in [20] for a Cuk converter, and in [21] for a power-factor-corrected isolated Cuk converter. Moreover, [22] presents a two-stage LCLC filter for interleaved AC–DC converters. For a three-phase active

Corresponding author:
Erdal Şehirli

E-mail:
esehirli@kastamonu.edu.tr

Received: January 6, 2023

Revision Requested: March 8, 2023

Accepted: July 14, 2023

Publication Date: January 31, 2024

DOI: 10.5152/electrica.2024.23001

bridge rectifier, an EMI filter is designed in [23] as well. [24] also presents the input current ripple estimation of multilevel grid-tied converters.

This paper presents the design and application of LCL, pi, LC with damping, and LC EMI filters for a boost converter operated in CCM. In the literature review, the design and analysis of the EMI filter effect on the boost converter are not included in the literature as presented in the paper, though it is a vital topic for a boost converter. In addition, the use of LCL filter with a boost converter is not presented in the literature in detail. For a boost converter including filters, this paper also derives a small-signal analysis. Furthermore, for a boost converter, filter influences on transfer functions are shown. Also, the frequency spectrum of the converter with filters is measured, and DM noises are investigated. Moreover, experimental verification is realized by a 15 W boost converter with a 25 kHz switching frequency. Applications and analysis prove that the LCL filter has better control characteristics. Further, the LC and Pi filters have better results in reducing DM noise. Besides, inductor reduction by 30% is maintained with the LCL filter. Also, simulation results support the application results.

II. BOOST CONVERTER

Fig. 1(a) shows the structure of a boost converter having an inductor, capacitor, power switch, diode, and load. Boost converters' output voltage is higher than the input voltage with the same polarity.

The operation and model of the boost converter can be derived via switch-off and -on equivalents, as shown in Fig. 1. At the on position of the switch, L is energized, and the load is fed by C. At the off position of the switch, L and the input supply deliver their energy to C and the load.

A mathematical model of the boost converter is derived by using Kirchhoff's law for switch-off and -on circuits in Fig. 1. For the switch-on equivalent, the model is obtained by (1–2) as in [14]. In the equations, V_{in} is the input voltage, V_o is the output voltage, C is the capacitance, L is the inductance, R is the load resistance, and i_L is the inductor current.

$$\frac{di_L}{dt}=\frac{V_{in}}{L} \tag{1}$$

$$\frac{dV_o}{dt}=-\frac{V_o}{RC} \tag{2}$$

For switch-off equivalent, a model is obtained by (3–4) as in [14, 19].

$$\frac{di_L}{dt}=\frac{V_{in}}{L}-\frac{V_o}{L} \tag{3}$$

$$\frac{dV_o}{dt}=\frac{i_L}{C}-\frac{V_o}{RC} \tag{4}$$

A boost converter model is presented in (7) with the form of (5) by using the average model concept in (6) as in [14]. In the equations, A is the system matrix, u is V_{in}, d is the duty cycle, and B is the input matrix.

$$\dot{x}=Ax+Bu \tag{5}$$

$$B=dB_1+(1-d)B_2\,,\ A=dA_1+(1-d)A_2\,, \tag{6}$$

$$\dot{x}=\begin{bmatrix}0 & \frac{-1+d}{L}\\ \frac{1-d}{C} & \frac{-1}{RC}\end{bmatrix}x+\begin{bmatrix}\frac{1}{L}\\ 0\end{bmatrix}u \tag{7}$$

The effect of EMI filters on boost converters can be analyzed using linear techniques; therefore, a boost converter model in (7) should be linearized. Linearization is done by using small-signal analysis, meaning linearization for the operation point. To obtain the small-signal model, (8) is used with (7), as in [14, 19, 20].

$$\dot{\tilde{x}}=\left(\bar{D}A_1+(1-\bar{D})A_2\right)\tilde{x}+\left((A_1-A_2)\bar{x}+(B_1-B_2)u\right)\tilde{d} \tag{8}$$

In (8), $d=\bar{D}+\tilde{d}$ and $x=\bar{x}+\tilde{x}$. Also, $\tilde{()}$, $\bar{()}$ symbols refer to small-signal variations and steady-state values. After small-signal analysis in (8), the converter transfer function can be acquired in (10) via using (9) as in [25].

$$T(s)=C(sI-A)^{-1}B \tag{9}$$

$$T(s)=\frac{\tilde{V}_0}{\tilde{d}}=\frac{-s\frac{V_{in}}{(1-d)^2RC}+\frac{V_{in}}{LC}}{s^2+\frac{s}{RC}+\frac{(1-d)^2}{LC}} \tag{10}$$

The minimum capacitor and inductor values for the CCM operation of the converter are designed by (11–12) as in [1]. In the equations, f_s is the switching frequency and ΔV_c is the capacitor ripple voltage.

$$L_{min}\geq\frac{D(1-D)^2R}{2f_s} \tag{11}$$

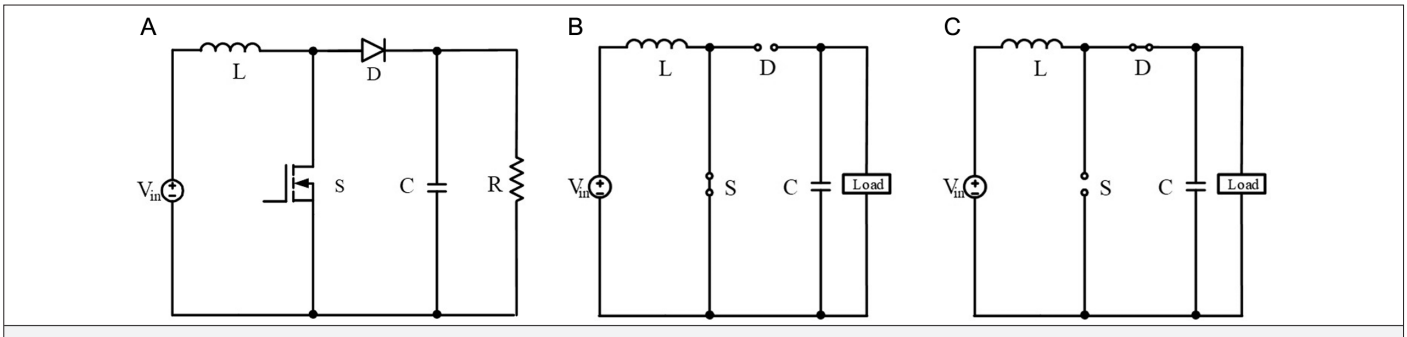

Fig. 1. (A) Boost DC–DC converter. (B) Switch-on equivalent. (C) Switch-off equivalent.

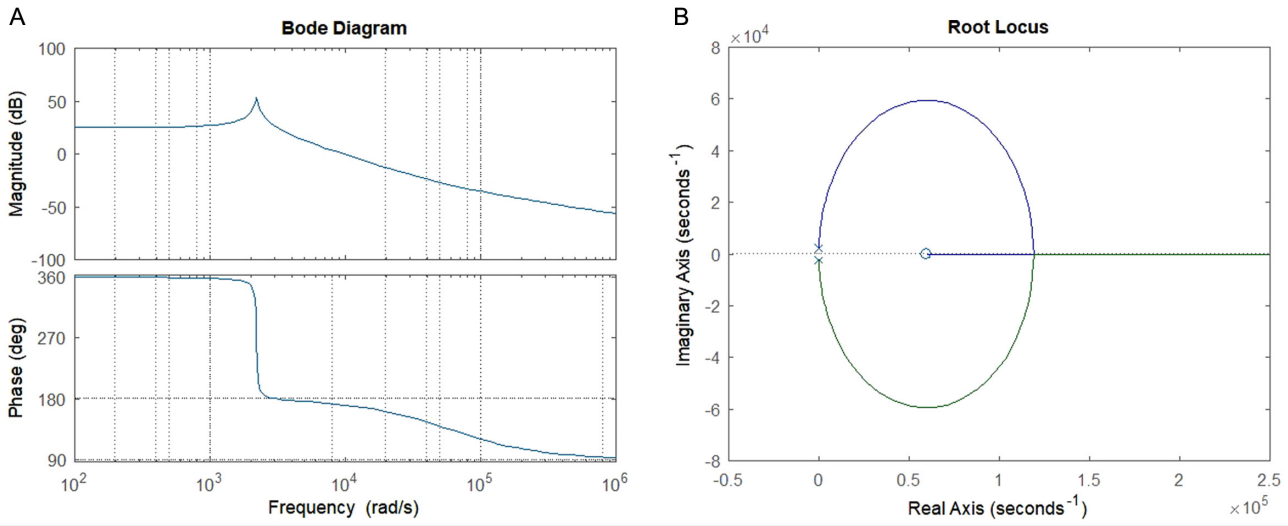

Fig. 2. (A) Bode. (B) Root locus diagram of boost converter.

$$C_{min}=\frac{DV_o}{f_sR\Delta V_c} \tag{12}$$

By using $L=147$ μH, $C=940$ μF, $R=13$ Ω, $V_{in}=12$ V, and $d=0.18$, Fig. 2 depicts root locus and bode diagrams. In the diagrams, the converter has a zero at 5.95×10^4 in the right half plane, meaning it has non-minimum phase characteristic. The poles are at $-40.9\pm 2.21\times10^3$ j. By increasing the controller gain, one pole will reach zero in the right half plane, and the other pole will reach infinity through the positive x axis, making the converter unstable. Also, increasing the gain by more than 0.0561 makes the system unstable.

III. ELECTROMAGNETIC INTERFERENCE FILTERS

Electromagnetic interference filters are connected between the power converter and the input source in order to diminish high-frequency noise and obtain continuous input current when the converter has a high ripple current. This paper investigates, designs, and implements LCL, LC with damping, pi, and LC filters shown in Fig. 3.

Furthermore, the filter effect on the converter is investigated by root locus and bode plots. Also, frequency spectrums are compared.

A. Inductor Capacitor Electromagnetic Interference

Fig. 3(a) gives the LC filter, including the inductor L_f capacitor C_f. Inductors and capacitors of the filter are chosen by using (13–14) as in [5, 6, 20].

$$f_o=\frac{1}{2\pi\sqrt{L_fC_f}},f_o=0.1f_s \tag{13}$$

$$L_f=\frac{(V_{in}-V_0)D}{\Delta I_{Lf}f_{sw}}, \tag{14}$$

Besides, (15) gives the filter transfer function.

$$T(s)=\frac{V_0}{V_{in}}=\frac{1}{(s^2L_fC_f+1)} \tag{15}$$

B. Inductor Capacitor with Damping Electromagnetic Interference Filter

Fig. 3(b) gives LC with a damping filter having an inductor L_f, capacitor C_f and a damping resistor R_b and capacitor C_b. Passive components of the filter are calculated by using (13–14, 16–17) as in [5, 6, 20]. n is the capacitance ratio, P_o is the converter output power, R_{in} is the input impedance of the converter, and ζ is the damping ratio.

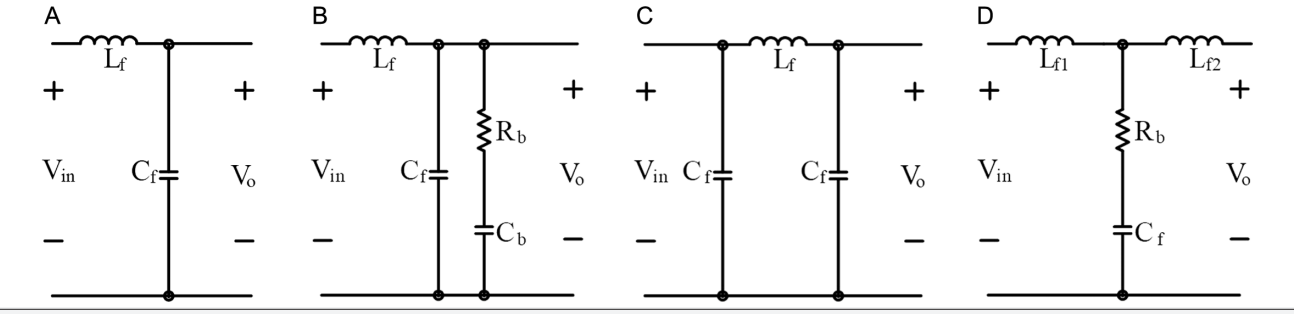

Fig. 3. Electromagnetic interference filters: (A) LC filter, (B) LC with damping, (C) pi filter, and (D) LCL filter.

$$\zeta=\frac{n+1}{n}\frac{L_f}{2R_b\sqrt{L_fC_f}},\quad n=C_D/C_f \tag{16}$$

$$\frac{L_f}{C_fR_b}\ll R_{in},\quad R_{in}=-V_{in}^2/P_o \tag{17}$$

Besides, (18) gives the filter transfer function.

$$T(s)=\frac{V_0}{V_{in}}=\frac{sR_bC_b+1}{s^3R_bC_bC_fL_f+s^2\left(R_dC_fL_f+R_bC_bL_f\right)+sR_bC_b+1} \tag{18}$$

C. Pi Electromagnetic Interference Filter

A pi filter is shown in Fig. 3(c), which has inductor L_f and two capacitors C_f. Passive components of the filter are calculated by using (13–14) as in [5, 6]. In addition to neglecting the input impedance, a pi filter has the same transfer function as the LC filter given in (19).

$$T(s)=\frac{V_0}{V_{in}}=\frac{1}{(s^2L_fC_f+1)} \tag{19}$$

D. Inductor-Capacitor-Inductor Electromagnetic Interference Filter

Inductor-capacitor-inductor electromagnetic interference filter is given in Fig. 3(d), having two inductors L_{f1}, $L_{f2,}$ capacitor $C_{f,}$ and a damping resistor R_b. Filter components are found in (13–14, 20–21), as in [9, 19, 20]. f_g is the grid frequency that is equal to "0," f_o is the filter resonance, and *r* is the inductance ratio.

$$f_o=\frac{1}{2\pi}\sqrt{\frac{L_{f1}+L_{f2}}{L_{f1}+L_{f2}C_f}},10f_g<f_o<0.5f_s,L_{f2}=rL_{f1} \tag{20}$$

$$R_b=\frac{1}{6\pi f_oC_f} \tag{21}$$

Besides, the transfer function of the filter is derived in (22). In (22), L_{f2} is assumed to be added to the L of the boost converter.

$$T(s)=\frac{V_0}{V_{in}}=\frac{C_fR_bs+1}{\left(s^2L_fC_f+R_bC_fs+1\right)} \tag{22}$$

IV. APPLICATIONS

A boost converter is experimentally verified by using LCL, pi, LC with damping, and LC filter in laboratory, as shown in Fig. 4(a). Also, simulations are conducted using power electronics simulator (PSIM) software, whose circuit is given in Fig. 4(b). Measurements are realized through the TPS2024B oscilloscope (Tektronix, Beaverton, OR, USA), TPP0201 voltage probes, and A622 current probe (Tektronix), as shown in Fig. 4a. Via the line impedance stabilizer network (LISN) in Fig. 4(a), DM noise is measured as in [20]. In LISN of Fig. 4(a), there are two 50μH inductors connected in series to the (+), (−) terminals of the DC power supply. Measurements on the 1.25 MHz scale are conducted by a 1 kΩ resistor that is connected in series with a 100 nF capacitor at the output of the LISN inductors, and at the input of the LISN, a 1 μF capacitor is connected. The LISN is tied between the power supply and filters. Furthermore, the hardware prototype shown in Fig. 4(a) includes a boost DC–DC converter, EMI filters, two DC power supplies (one for the converter and another one for the driver IC), and a dsPIC30F4011 microcontroller unit, which is used to control the converter.

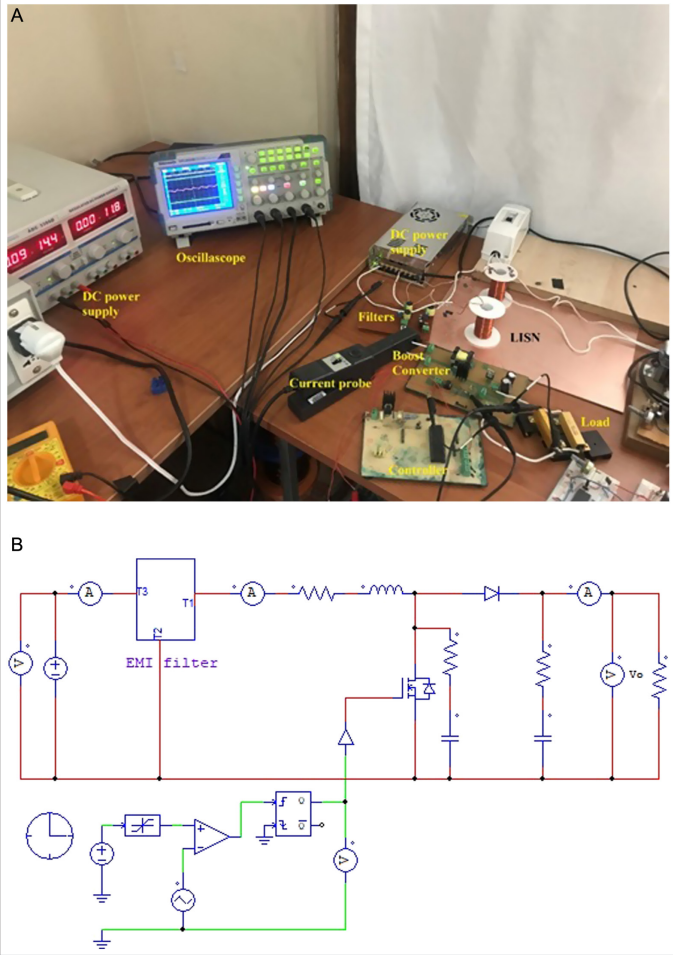

Fig. 4. (A) Laboratory set-up. (B) Simulation circuit.

Table I gives the passive component values used for the study.

A. Inductor Capacitor Electromagnetic Interference Filter

For showing filter influence to the converter, (15) is added to (10) to have a total transfer function in (23).

$$T(s)=\frac{\tilde{V}_0}{\tilde{d}}=\frac{-1460s+8.68\times10^7}{4\times10^{-9}s^4+3.27\times10^{-7}s^3+1.0195s^2+81.83s+4.87\times10^6} \tag{23}$$

TABLE I PASSIVE VALUES

Filter	L_f (L_{f1})	L_{f2}	C_f	R_d	C_d
LC	100 μH	-	40 μF	-	-
LC with damping	100 μH	-	40 μF	2.8 Ω	160 μF
pi	100 μH	-	40 μF	-	-
LCL	35 μH	35 μH	10 μF	0.44 Ω	-
Boost converter					
$L=147$ μH	$C=940$ μH		$d=0.18$	$f=25$kHz	$R=13$ Ω

C: Capacitor, L: inductor.

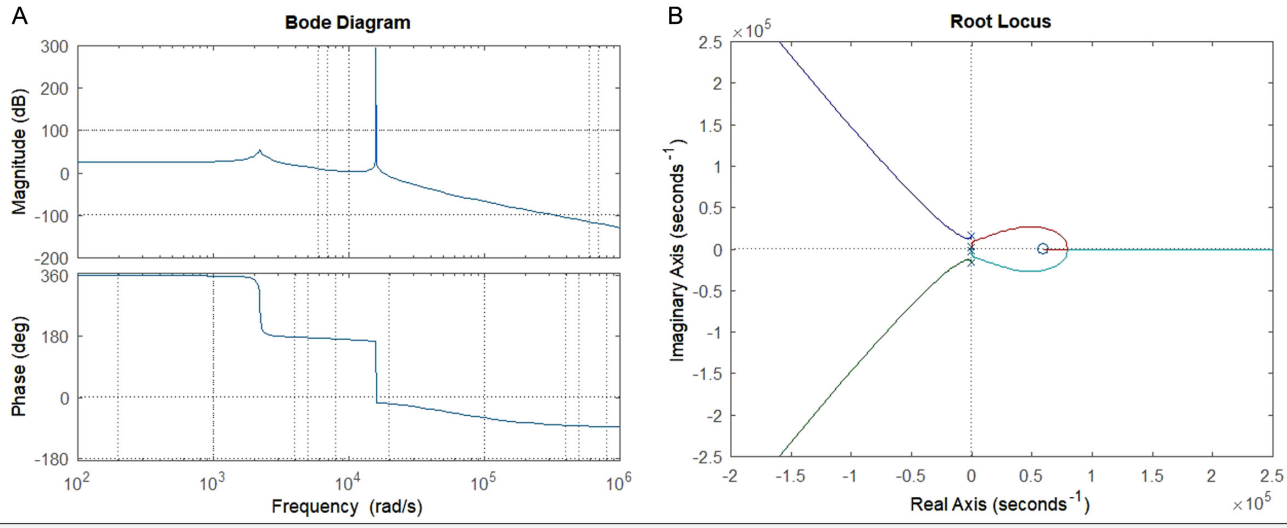

Fig. 5. (A) Bode diagram. (B) Root locus diagram of inductor capacitor filter with a boost converter.

The filter effect is observed via the bode and root locus graphs depicted in Fig. 5. In the root locus graph, two poles are added because of the LC filter. A boost converter with filter is still non-minimum phase, having a zero at 5.95×10^4 in the right half plane. The pole locations are $\pm 1.58 \times 10^4$j and $-40.9 \pm 2.21 \times 10^3$j. The system is unstable after incrementing the controller gain by more than 0.0539.

Furthermore, Fig. 6 shows application and simulation results, including L_1 current, output–input current, Pulse width modulation (PWM), and input–output voltage. A continuous inductor current with a higher ripple for CCM is observed. From the application, I_{L1} stays between 1.8 and 1.1 A. I_{in} is between 1.52 and 1.4A. I_o is between 1.32 and 1.1 A. V_{in} is 12.8 V, and V_o is 14.1 V. From simulation, I_{L1} stays

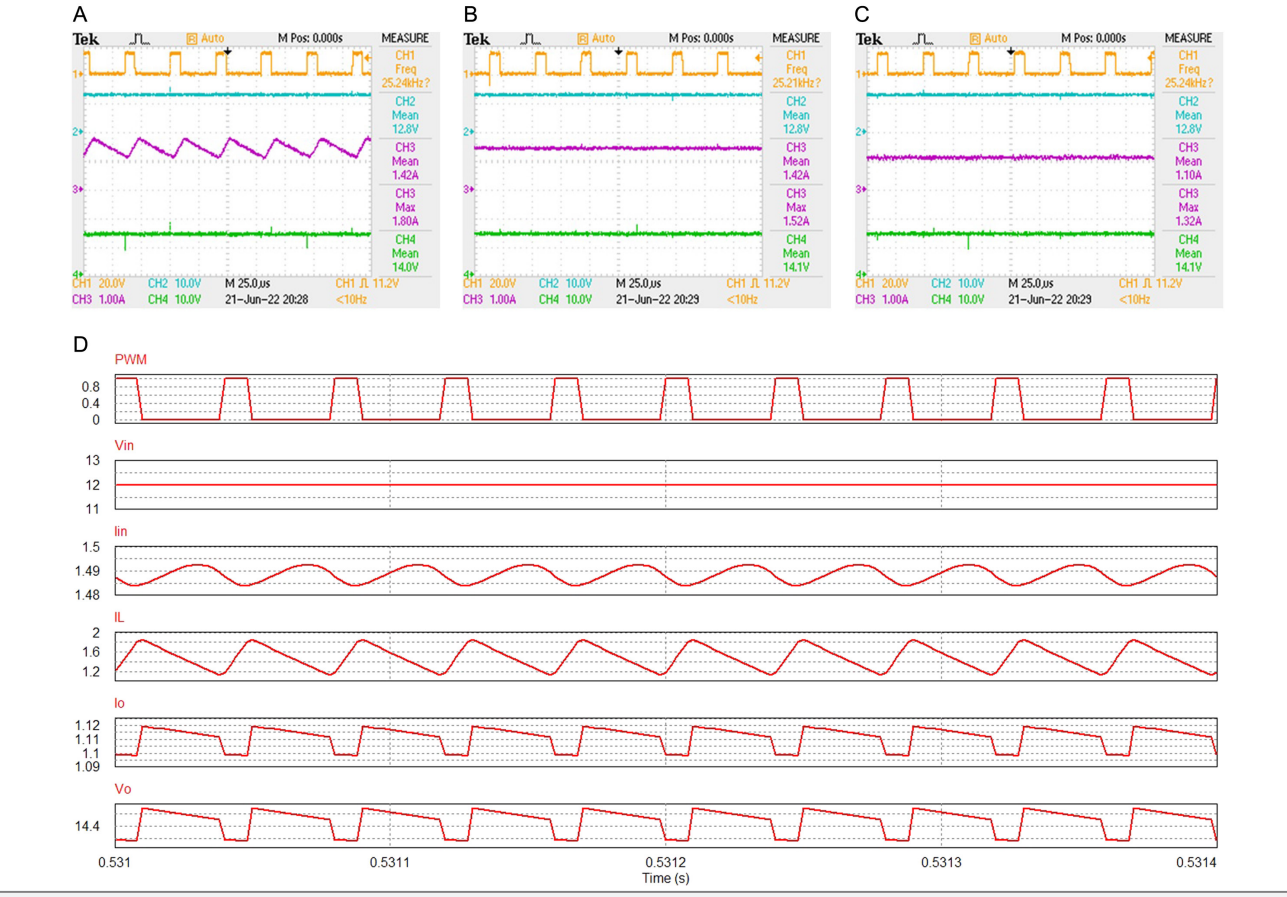

Fig. 6. (A) PWM, V_{in}, I_{L1}, V_o; (B) PWM, V_{in}, I_{in}, V_o, (C) PWM, V_{in}, I_o, V_o, and (D) simulation results with inductor capacitor filter.

Fig. 7. (A) I_{L1} at 25 kHz, (B) I_{in} at 25 kHz, (C) DM at 1.25 MHz, and (D) FFT simulation results with inductor capacitor filter.

between 1.858 and 1.1192 A. I_{in} is between 1.49256 and 1.4838 A. I_o is between 1.11925 and 1.09824 A. V_{in} is 12V. V_o is between 14.55 and 14.277 V.

Besides, the converter frequency spectrum using the LC filter is given in Fig. 7. Fig. 7(a) shows the L_1 current frequency spectrum; Fig. 7(b) shows the input current frequency spectrum at 25 kHz scale; Fig. 7(c) shows the frequency spectrum of DM noise at 1.25 MHz scale; and Fig. 7(d) shows the Fast fourier transform(FFT) simulation. It is seen that the input current has 16 dB at 25 kHz, 15 dB at 124 kHz, and 14 dB at 174 kHz magnitude. Also, DM noises are 12 dB at 0.375 MHz, 20 dB at 3.8 MHz, and 19 dB at 10.6 MHz. From FFT simulation, I_{in} is 1.50657 A at (0 Hz), 0.00417 A at (25 kHz), and 0.00055 A at (50 kHz). I_L is 1.5034 A at (0 Hz), 0.294 A at (25 kHz), 0.0946 A at (50 kHz), 0.02534 A at (75 kHz), and 0.0054 A at (125 kHz).

B. Inductor Capacitor with Damping Electromagnetic Interference Filter

Considering (18) and (10), a cascaded transfer function is organized in (24) to show the filter effect.

$$T(s)=\frac{\tilde{V_0}}{\tilde{d}}=\frac{-0.6543s^2+3.74\times10^4 s+8.68\times10^7}{1.792\times10^{-12}s^5+5.61410^{-8}s^4+0.00046130s^3+1.309s^2+2262s+4.866\times10^6} \quad (24)$$

By using the transfer function in (24), root locus and bode graphs are sketched in Fig. 8 for a boost converter employing an LC with a damping filter. It is observed that three poles and a zero are added to the converter by the filter at -2.03×10^4, -7.09×10^3, -3.88×10^3, and -2.23×10^3 by the root locus graph. The converter poles and zero are at $-40.9\pm2.21\times10^3$ j and at 5.95×10^4. Increasing the controller gain by more than 0.009 makes the system unstable.

Furthermore, Fig. 9 shows application and simulation results, including L_1 current, input–output currents, PWM, input voltage, and output voltage. A continuous inductor current with a higher ripple for CCM is observed. From the application, I_{L1} stays between 1.8 and 1.1A. I_{in} is between 1.56 and 1.4A. I_o is between 1.24 and 1.1A. V_{in} is 12.8V. V_o is 14.1V. From simulation, I_{L1} stays between 1.8578 and 1.11935A. I_{in} is between 1.492285 and 1.484A. I_o is between 1.119248 and 1.09824A. V_{in} is 12V, and V_o is between 14.55 and 14.277V.

Besides, Fig. 10(a) shows L_1 current frequency spectrum, Fig. 10(b) shows input current frequency spectrum at 25kHz scale, and Fig. 10(c) shows frequency spectrum of DM noise at 1.25 MHz scale. Fig. 10(d) shows FFT simulation. It is seen that the input current has 14 dB at 25 kHz, 13.6 dB at 124 kHz, and 16 dB at 174 kHz magnitude. Also, DM noises are 25 dB at 0.375 MHz, 21 dB at 3.8 MHz, and 20 dB at 10.6 MHz. From FFT simulation, I_{in} is 1.5084 A at (0 Hz), 0.00394 A

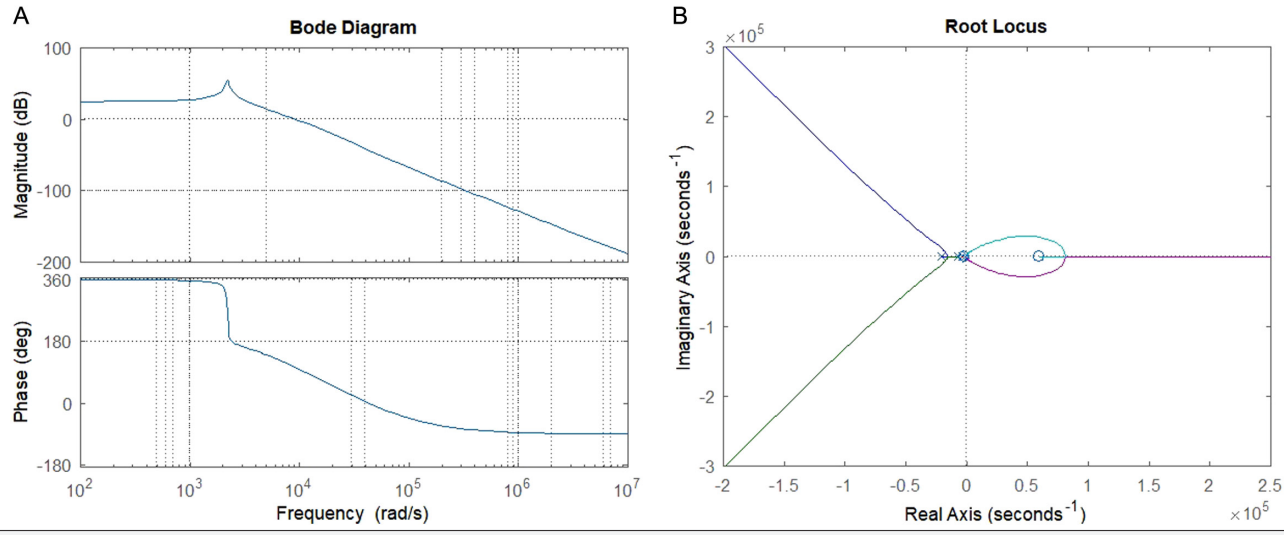

Fig. 8. (A) Bode diagram. (B) Root locus diagram of inductor capacitor with damping filter with boost converter.

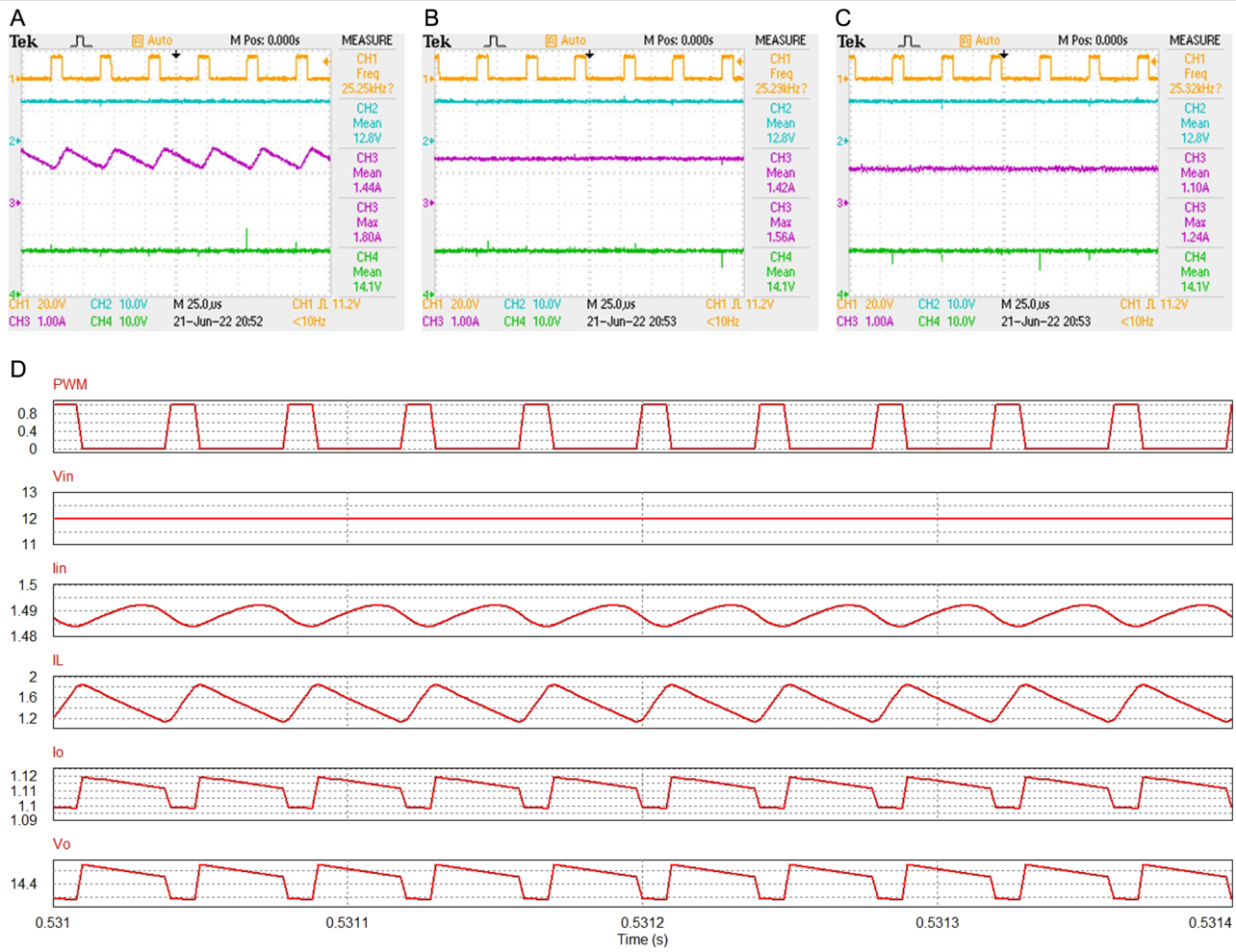

Fig. 9. (A) PWM, V_{in}, I_{L1}, V_o; (B) PWM, V_{in}, I_{in}, V_o, (C) PWM, V_{in}, I_o, V_o, and (D) simulation results with inductor capacitor with damping filter.

Fig. 10. (A) I_{L1} at 25 kHz, (B) I_{in} at 25 kHz, (C) DM at 1.25 MHz, and (D) FFT simulation results with inductor capacitor with damping filter.

at (25 kHz), 0.000519 A at (50 kHz). I_L is 1.50338 A at (0 Hz), 0.294 A at (25 kHz), 0.09458 A at (50 kHz), 0.02534 A at (75 kHz), and 0.0054 A at (125 kHz).

C. Pi Electromagnetic Interference Filter

By omitting the source impedance, an LC filter transfer function is employed for a pi filter. So, bode and root locus diagrams are the same as with an LC filter in Fig. 5. In Fig. 11, L_1 current, input current, output current, PWM, and input–output voltage are given. Also, continuous inductor current with a higher ripple is observed for CCM. From application, I_{L1} stays between 1.8 and 1.1 A. I_{in} is between 1.68 and 1.4 A. I_o is between 1.24 and 1.1 A. V_{in} is 12.8 V. V_o is 14.1V. From simulation, I_{L1} stays between 1.858 and 1.11918 A. I_{in} is between 1.49256 and 1.4838 A. I_o is between 1.11925 and 1.09824 A. V_{in} is 12 V. V_o is between 14.55 and 14.277 V.

Besides, Fig. 12(a) shows application and simulation results, including the frequency spectrum of L_1 current; Fig. 12(b) shows the frequency spectrum of input current at 25 kHz scale; Fig. 12(c) shows frequency spectrum of DM noise at 1.25 MHz scale; and Fig. 12(d) shows FFT simulation. It is seen that the input current has 12 dB at 25 kHz, 11 dB at 124 kHz, and 13 dB at 174 kHz magnitude. Also, DM noises are 20 dB at 0.375 MHz, 20 dB at 3.8 MHz, and 19 dB at 10.6 MHz. From the FFT simulation, I_{in} is 1.507 A at (0 Hz), 0.003747 A at (25 kHz), and 0.000485 A at (50 kHz). I_L is 1.5034 A at (0 Hz), 0.294 A at (25 kHz), 0.0946 A at (50 kHz), 0.02534 A at (75 kHz), and 0.0054 A at (125 kHz).

D. Inductor-Capacitor-Inductor Electromagnetic Interference Filter

Inductor-capacitor-inductor filter is applied to a boost converter by using the values given in Table I. Although in the literature, LCL filters are commonly used for inverter topologies, LCL filters for boost converters are not presented in detail.

The transfer function is rearranged in (25) by cascading (10) and (22) to present the influence of the filter on the converter.

$$T(s)=\frac{\tilde{V_0}}{\tilde{d}}=\frac{0.0064s^2+1769s+7.01\times10^7}{3.5\times10^{-10}s^4+4.43\times10^{-6}s^3+1.0017s^2+99.13s+3.93\times10^6} \quad (25)$$

By using (25), Fig. 13 depicts bode and root locus graphs. By root locus graph, the system has two zeros and four poles located at $-4.8\text{x}10^4$, $-2.27\text{x}10^5$, $-6.29\text{ x }10^3 \pm 5.31\text{ x }10^4$j, and $-40.9 \pm 1.98\text{ x }10^3$ j, respectively. The system is unstable if the controller gain increases by more than 6.1349.

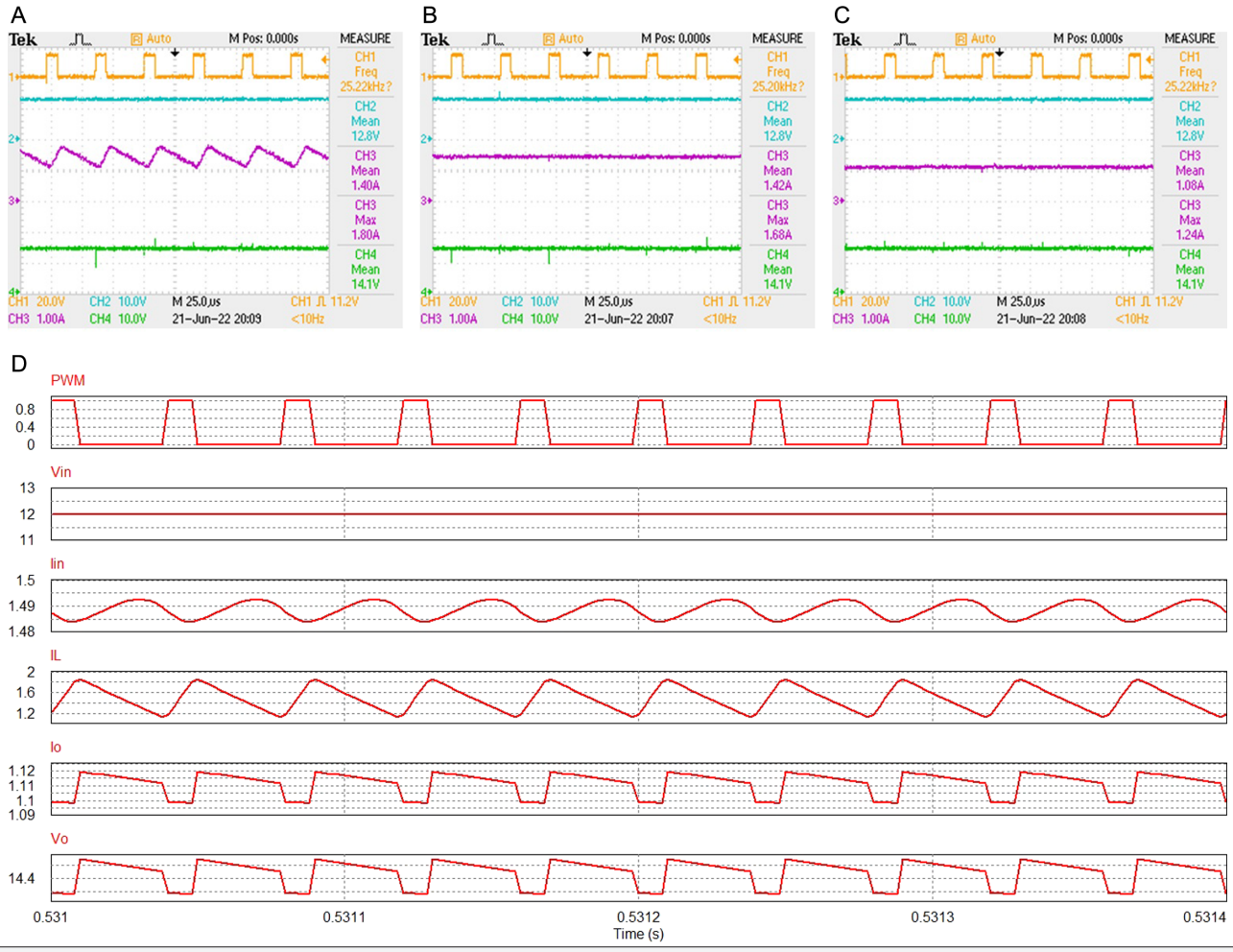

Fig. 11. (A) PWM, V_{in}, I_{L1}, V_o, (B) PWM, V_{in}, I_{in}, V_o, (C) PWM, V_{in}, I_o, V_o, and (D) simulation results with a pi filter.

Furthermore, Fig. 14 shows application and simulation results, including L_1 current, input–output current, PWM, input voltage, and output voltage. Continuous input current is acquired. From the application, I_{L1} stays between 1.76 and 1.2A. I_{in} is between 1.52 and 1.4A. I_o is between 1.4 and 1A but it stays at 0.2A. V_{in} is 12.8V. V_o is 14.1V. From simulation, I_{L1} stays between 1.792 and 1.18865A. I_{in} is between 1.526 and 1.446A. I_o is between 1.11852 and 1.098A. V_{in} is 12V. V_o is between 14.54 and 14.277V.

Besides, Fig. 15(a) shows the L_1 current frequency spectrum, Fig. 15(b) shows the input current frequency spectrum at 25 kHz scale, and Fig. 15(c) shows the frequency spectrum of DM noise at 1.25 MHz scale. Fig. 15(d) shows the FFT simulation. It is seen that the input current has 24 dB at 25 kHz, 18 dB at 124 kHz, and 14 dB at 174 kHz magnitude. Also, DM noises are 30 dB at 0.375 MHz, 18 dB at 3.8 MHz, and 22 dB at 10.6 MHz. From FFT simulation, I_{in} is 1.506 A at (0 Hz), 0.03815 A at (25 kHz), and 0.00416 A at (50 kHz). I_L is 1.504 A at (0 Hz), 0.2415 A at (25 kHz), 0.07677 A at (50 kHz), 0.0205 A at (75 kHz), and 0.0043 A at (125 kHz).

V. RESULTS AND FINDINGS

Filter comparison, including maximum control gain, filter attenuation, and peak magnitude, is given in Table II by using the transfer functions in (23), (24), and (25). As a result, the LCL filter gives better results for controller gain and peak magnitude, while the LC and Pi give better results for filter attenuation.

Differential mode noise comparisons of filters are presented in Table III. As shown in Table III, the pi filter gives better results for 25 kHz, 124 kHz, and 174 kHz. The inductor capacitor filter for 0.375 MHz and 10.6 MHz and the LCL filter for 3.8 MHz present better results. In addition, the FFT simulation results are summarized in Table IV. It is observed that the LCL filter gives poorer attenuation results at 25 kHz and 50 kHz by ten times than other filters, similar to the results in Table III at lower frequencies.

As a result of the simulations, the LC, LC with damping, and pi filters have the same I_{in}, I_L, and V_o values, but the LCL filter has higher ripple values than the other filter structures. Also, in experiments, similar results with simulations are obtained. Besides, experimental results are slightly different than simulation results, up to a maximum 6.7%. The results of the filter regarding simulations and experiments are given in Table V.

VI. CONCLUSION

This paper designs an LCL, pi, LC with damping, and LC EMI filter for a boost converter operated in CCM. Filter effects on control

Fig. 12. (A) I_{L1} at 25 kHz, (B) I_{in} at 25 kHz, (C) DM at 1.25 MHz, and (D) FFT simulation results with a pi filter.

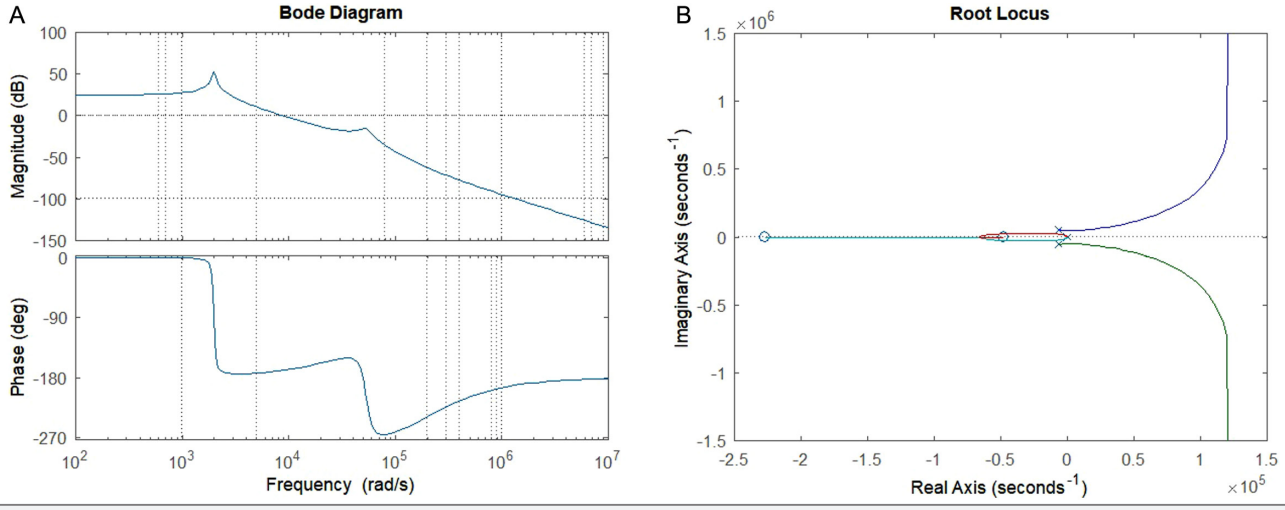

Fig. 13. (A) Bode diagram. (B) Root locus diagram of inductor-capacitor-inductor filtered boost converter.

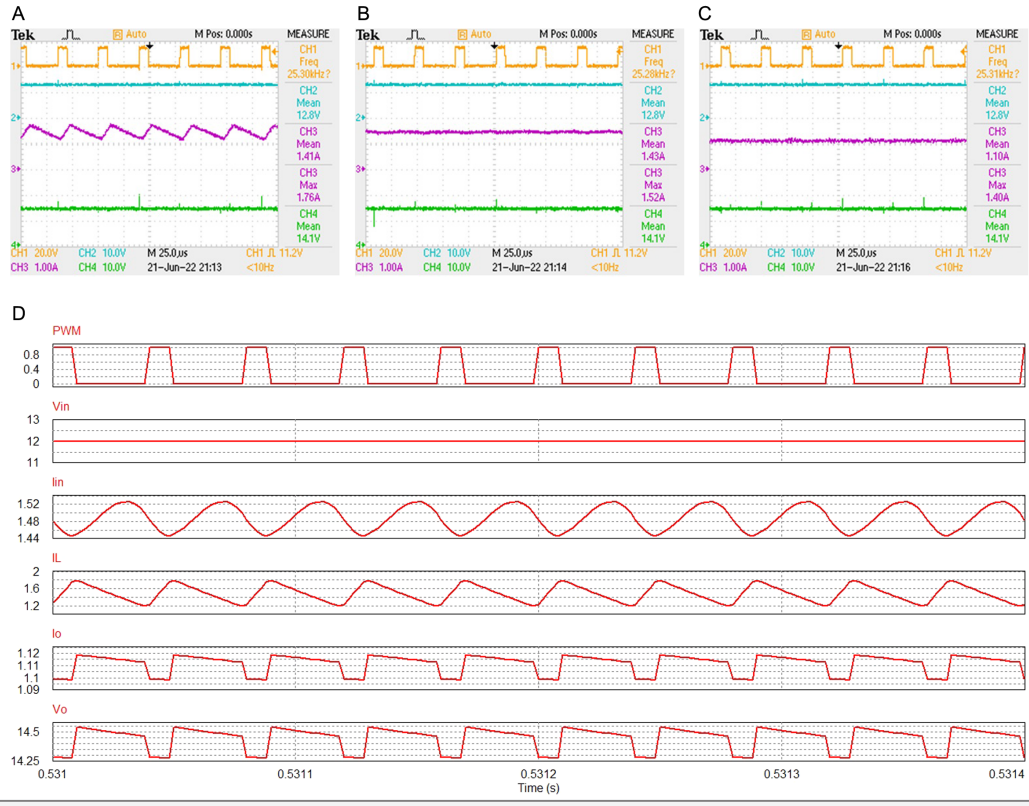

Fig. 14. (A) PWM, V_{in}, I_{L1}, V_o; (B) PWM, V_{in}, I_{in}, V_o, (C) PWM, V_{in}, I_o, V_o, and (D) simulation results with LCL filter.

Fig. 15. (A) I_{L1} at 25 kHz, (B) I_{in} at 25 kHz, (C) DM at 1.25 MHz, and (D) FFT simulation results with inductor-capacitor-inductor filter.

TABLE II COMPARISON OF FILTERS

	LC	LC with damping	Pi	LCL
Control gain	0.0539	0.009	0.0539	6.1349
Filter attenuation by decade (10^5–10^6 rad/s)	61.7 dB	61.3 dB	61.7 dB	51.3 dB
Peak magnitude at corner frequency	295 dB at 1.58×10^4 rad/s	54.9 dB at 2.21×10^3 rad/s	295 dB at 1.58×10^4 rad/s	52.7 dB at 1.98×10^3 rad/s

C: Capacitor, L: inductor.

TABLE III DIFFERENTIAL MODE NOISES OF FILTERS

LC	LC with damping	Pi	LCL
16 dB at 25 kHz	14 dB at 25 kHz	12 dB at 25 kHz	24 dB at 25 kHz
15 dB at 124 kHz	13.6 dB at 124 kHz	11 dB at 124 kHz	18 dB at 124 kHz
14 dB at 174 kHz	16 dB at 174 kHz	13 dB at 174 kHz	14 dB at 174 kHz
12 dB at 0.375 MHz	25 dB at 0.375 MHz	20 dB at 0.375 MHz	22 dB at 0.375 MHz
20 dB at 3.8 MHz	21 dB at 3.8 MHz	20 dB at 3.8 MHz	18 dB at 3.8 MHz
19 dB at 10.6 MHz	20 dB at 10.6 MHz	19 dB at 10.6 MHz	30 dB at 10.6 MHz

TABLE IV FFT SIMULATION RESULTS OF FILTERS

	LC	LC with damp.	Pi	LCL
I_{in} (A)	1.50657 (0 Hz)	1.5084 (0 Hz)	1.507(0 Hz)	1.506 (0 Hz)
	0.00417 (25 kHz)	0.00394 (25 kHz)	0.003747 (25 kHz)	0.03815 (25 kHz)
	0.00055 (50 kHz)	0.000519 (50 kHz)	0.000485 (50 kHz)	0.00416 (50 kHz)
I_L (A)	1.5034 (0 Hz)	1.50338 (0 Hz)	1.5034 (0 Hz)	1.504 (0 kHz)
	0.294 (25 kHz)	0.294 (25 kHz)	0.294 (25 kHz)	0.2415 (25 kHz)
	0.0946 (50 kHz)	0.09458 (50 kHz)	0.0946 (50 kHz)	0.07667 (50 kHz)
	0.02534 (75 kHz)	0.02534 (75 kHz)	0.02534 (75 kHz)	0.0205 (75 kHz)
	0.0054 (125 kHz)	0.0054 (125 kHz)	0.0054 (125 kHz)	0.0043 (125 kHz)

and DM noise are not presented in the literature, even though an EMI filter is vital for a boost converter. Also, the design of the LCL filter for the boost converter is not proposed in the literature in detail. This article presents a practical EMI filter design method that is a generally complex phenomenon in power electronics for a boost DC–DC converter. Furthermore, the transfer function, small-signal analysis, and mathematical model of the boost converter for CCM are summarized. Also, the impact of each filter on the boost converter is investigated by bode diagrams and root locus.

The study is carried out through experiments with a 15 Watt converter and simulations. As a result of the experiments, frequency spectrums, input–output voltages, and currents are given for each filter. It is observed by the application results that, regarding control characteristics, the LCL filter gives better results. Also, for DM noise reduction, the LC and pi filters are better than other topologies. With respect to FFT simulation, although at higher frequencies the LCL filter has higher values at the input current, it has lower values at the inductor current. Besides, similar efficiencies are obtained by each filter at 84%. Moreover, the LCL filter reduces the filter inductor amount by 30% compared other topologies. Further, regarding inductor current ripple, the LCL filter has a lower value compared to other structures with regard to both simulation and experimental results. In terms of input current ripple, the LCL and LC filters have lower ripple at experiments, while the LCL filter has higher ripple at simulations. In addition, according to simulation results, the LCL filter has lower output voltage and output current ripples. Other filter topologies have the same voltage and current ripples in simulations. However, the output current ripple of the LCL filter is relatively higher than other topologies in experiments. Moreover, in applications, each filter except the LCL filter has the same ripple values on the input inductor current. The LC filter also has a lower input current ripple than the pi and LC with damping filters. Furthermore, the pi and LC with damping filters have a lower input current ripple than the pi and LC with damping. Furthermore, pi and LC with damping filters have a lower output current ripple than other types.

TABLE V. SIMULATION AND EXPERIMENTAL RESULTS OF FILTERS

	Simulation				Experiment			
	LC	LC with damp.	Pi	LCL	LC	LC with damp.	Pi	LCL
I_{in} (A)	1.49256–1.4838	1.492285–1.484	1.49256–1.4838	1.526–1.446	1.52–1.4	1.56–1.4	1.68–1.4	1.52–1.4
I_L (A)	1.858–1.1192	1.8578–1.11935	1.858–1.11918	1.792–1.18865	1.8–1.1	1.8–1.1	1.8–1.1	1.76–1.2
I_o (A)	1.11925–1.09824	1.119248–1.09824	1.11925–1.09824	1.11852–1.098	1.32–1.1	1.24–1.1	1.24–1.1	1.4–1
V_{in} (V)	12	12	12	12	12.8	12.8	12.8	12.8
V_o (V)	14.55–14.277	14.55–14.277	14.55–14.277	14.54–14.277	14.1	14.1	14.1	14.1

Peer-review: Externally peer-reviewed.

Declaration of Interests: The author has no conflict of interest to declare.

Funding: The author declared that this study has received no financial support.

REFERENCES

1. M. K. Kazimierczuk, *Pulse-Width Modulated DC-DC Power Converters*. Singapore: Wiley, 2008.
2. R. W. Erickson, "Optimal single resistor damping input filters," Fourteenth Annual Applied Power Electronics Conference and Exposition, Dallas, USA, 1999, pp. 1073–1079.
3. J. Wys, and J. Biela, "EMI DM filter volume minimization for a PFC Boost converter including Boost inductor variation and MF EMI limits," 17th European Conference on Power Electronics and Applications. Geneva, Switzerland: Appl, 2015, pp. 1–10. [CrossRef]
4. D. M. Mitchell, "Power line filter design considerations for DC-DC converters," *IEEE Ind. Appl. Mag.*, vol. 5, no. 6, pp. 16–26, 1999. [CrossRef]
5. F. Hammerle, "*Input impedance measurements for stable input-filter design*," By Florian Hämmerle. Klaus, Aut., 2017. https://www.omicron-lab.com/fileadmin/assets/Bode_100/ApplicationNotes/Input_Impedance/AppNote_InputImpedance_V1.0.pdf
6. M. Sclocchi, *Input Filter Design for Switching Power Supplies*. Dallas, USA: Texas Instr, 2011.
7. H. Li, Y. Ding, Z. Yang, and Y. Jiang, "Optimization design of EMI filter with chaotic PWM in DC-DC converters," IEEE Workshop on Wide Bandgap Power Devices and Applications in Asia, Taipei, Taiwan, 2019, pp. 1–6. [CrossRef]
8. J. He, Y. Liu, C. Wang, and L. Cao, "Magnetic coupling common mode conducted EMI analysis and Improvement in a Boost converter," *MDPI World Electr. Veh. Jour*, vol. 12, no. 4, pp. 2–10, 2021. [CrossRef]
9. A. E. W. H. Kahlane, L. Hassaine, and M. Kherchi, "LCL filter design for photovoltaic grid connected systems," *Revue Des Energies Renouvelables*, 2014, pp. 227–232. (Conference paper) https://www.cder.dz/download/sienr2014_31.pdf
10. J. M. Sosa, G. Escobar, P. R. Panfilo, G. Vazquez, M. A. Juarez, and J. C. Nava-Cruz, "A model based controller for a DC-DC Boost converter with an LCL input filter," 41st Annual Conference of the IEEE Industrial Electronics Society., Yokohama, Japan, 2015, pp. 619–624. [CrossRef]
11. R. Roy, and S. Kapat, "Input filter-based ripple injection for mitigating limit cycling in buck converters driving CPL," *IEEE J Emerg. Select. Top. Pow Electron.*, vol. 9, no. 2, pp. 1315–1327, 2021. [CrossRef]
12. M. Wu, D. D. C. Lu, and C. K. Tse, "Direct and optimal linear active methods for stabilization of LC input filters and DC/DC converters under voltage mode control," *IEEE J. Emerg. Sel. Topics Circuits Syst.*, vol. 5, no. 3, pp. 402–412, 2015. [CrossRef]
13. M. U. Iftikhar, D. Sadarnac, and C. Karimi, "Conducted EMI suppression and stability issues in switch mode DC-DC converters," IEEE International Multitopic Conference, Islamaabad, Pakistan, 2006, pp. 389–394. [CrossRef]
14. H. A. Gawad, and V. K. Sood, "Small-signal analysis of Boost converter, including parasitic, operating in CCM," 6th IEEE Power India International Conference, Delhi, India, 2014, pp. 1–5.
15. M. Leng, G. Zhou, Q. Tian, G. Xu, and F. Blaabjerg, "Small signal modeling and design analysis for Boost Converter with valley V^2 control," *IEEE Trans. Power Electron.*, vol. 35, no. 12, pp. 13475–13487, 2020. [CrossRef]
16. B. Choi, S. S. Hong, and H. Park, "Modeling and small-signal analysis of controlled on-time Boost power-factor-correction circuit," *IEEE Trans. Ind. Electron.*, vol. 48, no. 1, pp. 136–142, 2001. [CrossRef]
17. B. Choi, S. S. Hong, and H. Park, "Modeling and small-signal analysis of controlled on-time Boost power factor correction circuit," Third International Power Electronics and Motion Control. Conference, Beijing, China, 2000, pp. 490–495.
18. K. Gorecki, and K. Detka, "Application of average electrothermal models in the SPICE-aided analysis of Boost converters," *IEEE Trans. Ind. Electron.*, vol. 66, no. 4, pp. 2746–2755, 2019. [CrossRef]
19. E. Şehirli, "Analysis of LCL filter topologies for DC-DC isolated Cuk converter at CCM operation," *IEEE Access*, vol. 10, pp. 113741–113755, 2022. [CrossRef]
20. E. Şehirli, "Examining the design of different types of DM EMI filters and their effect on EMI noise and control characteristics for Cuk DC-DC converter," *Int. Trans. Electr. Ener. Syst.*, vol. 2023, p. 1–18, 2023. [CrossRef]
21. E. Şehirli, "Examining the impacts of DM filters to PFC isolated Ćuk converter for DCM operation by comparing Si and SiC MOSFET," *Sci. Rep.*, vol. 13, no. 1, p. 4732, 2023. [CrossRef]
22. R. Phukan *et al.*, "Design of an indirectly coupled filter building block for modular interleaved AC–DC converters," *IEEE Trans. Power Electron.*, vol. 37, no. 11, pp. 13343–13357, 2022. [CrossRef]
23. M. J. Heller, F. Krismer, and J. W. Kolar, "EMI filter design for the integrated dual three-phase active bridge (D3AB) PFC rectifier," *IEEE Trans. Power Electron.*, vol. 37, no. 12, pp. 14527–14546, 2022. [CrossRef]
24. D. Biadene, "Spectrum estimation of input current ripple on a wide class of multilevel grid-tied converters," *IEEE Trans. Power Electron.*, vol. 38, no. 3, pp. 2855–2860, 2023. [CrossRef]
25. N. S. Nise, *Control Systems Engineering*. NJ, USA: Wiley, 2011.

Erdal Şehirli was born in Kastamonu, Turkey, in 1983. He received the first B.S. degree in electrical education from Gazi University in 2006, the second B.S. degree in electrical engineering from Istanbul Technical University in 2016, and the first M.S. degree in electrical education, the second M.S. degree in electrical engineering, and the Ph.D. degree in electricity education from Kocaeli University, Turkey, in 2009, 2016, and 2017, respectively. From 2009 to 2018, he was a Lecturer at the Vocational College of Higher Education, Kastamonu University. Since 2018, he has been an Assistant Professor with the Department of Electrical Engineering, Kastamonu University. His research interests include power electronics and control systems and microgrids.